



Magnetic Exchange Interactions in the Molecular Nanomagnet Mn_{12}

A. Chiesa,^{1,2} T. Guidi,³ S. Carretta,¹ S. Ansbro,^{4,5} G. A. Timco,⁴ I. Vitorica-Yrezabal,⁴ E. Garlatti,¹
G. Amoretti,¹ R. E. P. Winpenny,⁴ and P. Santini¹

¹*Dipartimento di Scienze Matematiche, Fisiche e Informatiche, Università di Parma, I-43124 Parma, Italy*

²*Institute for Advanced Simulation, Forschungszentrum Jülich, 52425 Jülich, Germany*

³*ISIS Facility, Rutherford Appleton Laboratory, OX11 0QX Didcot, United Kingdom*

⁴*School of Chemistry and Photon Science Institute, University of Manchester, M13 9PL Manchester, United Kingdom*

⁵*Institut Laue-Langevin, 71 Avenue des Martyrs CS 20156, Grenoble Cedex 9 F-38042, France*

(Received 14 July 2017; published 22 November 2017)

The discovery of magnetic bistability in Mn_{12} more than 20 years ago marked the birth of molecular magnetism, an extremely fertile interdisciplinary field and a powerful route to create tailored magnetic nanostructures. However, the difficulty to determine interactions in complex polycentric molecules often prevents their understanding. Mn_{12} is an outstanding example of this difficulty: although it is the forefather and most studied of all molecular nanomagnets, an unambiguous determination of even the leading magnetic exchange interactions is still lacking. Here we exploit four-dimensional inelastic neutron scattering to portray how individual spins fluctuate around the magnetic ground state, thus fixing the exchange couplings of Mn_{12} for the first time. Our results demonstrate the power of four-dimensional inelastic neutron scattering as an unrivaled tool to characterize magnetic clusters.

DOI: 10.1103/PhysRevLett.119.217202

The ability to store magnetic information in a single molecule was reported for the first time in the Mn_{12} polymetallic complex [1]. Many further breakthroughs followed from studies of this molecule, including the observation of macroscopic quantum tunneling of magnetization [2,3], and the discovery that it can be used to build devices based on the Grover algorithm [4]. The phrase “single-molecule magnet” was invented to describe the physics of Mn_{12} , and this molecule inspired the entire field of molecular magnetism, which continues to produce remarkable science [5–18]. However, the understanding of complex polycentric molecules is often limited by the difficulty to determine the interactions within the core. Mn_{12} is a particularly striking example: despite hundreds of papers, there is not even an unambiguous description for the leading interactions of this archetypal molecule, 25 years after it fathered a new field of science. Thus, the debate about Mn_{12} is still completely open, as witnessed by recent studies [19–21].

The phenomenology of molecular nanomagnets results from a number of interactions in the magnetic core, where isotropic exchange couplings are usually leading and various types of anisotropic one- and two-ion terms act perturbatively. The interplay of these interactions results in a multitude of physical behaviors, usually described in terms of simplified effective models. These are parametrized to capture distinctive low-temperature and low-frequency properties, but in many cases with complex cores the determination of the fundamental underlying spin Hamiltonian is still a challenge. Molecules displaying magnetic remanence like Mn_{12} are usually described in terms of phenomenological “giant spin” models, where a

single quantum spin S ($S = 10$ in Mn_{12}) represents the magnetic core as a whole [22,23]. Although this approach is cost effective in terms of model complexity, it leaves in the shadows the nature of the giant spin at the atomic level, hindering the tailoring of the magnetic core for improved performance in fundamental or applicative issues [24]. Moreover, the many-spin character of the core emerges already in the low-energy physics (see, e.g., [11,25]).

Here we exploit four-dimensional inelastic neutron scattering [8] to portray the spin precession patterns, which are unambiguous fingerprints of the magnetic Hamiltonian, and we thus pinpoint the exchange couplings of Mn_{12} for the first time. Our results open unprecedented prospects in understanding magnetic spin clusters and motivate the synthesis of new polycentric nanomagnets, where the set of interactions is optimal for specific fundamental issues or applications.

Most of the proposed models for Mn_{12} are based on a set of four isotropic exchange parameters, reported in the schematic representation in Fig. 1(a) (with $J_4 = J'_4$). The spin Hamiltonian also includes anisotropic terms accounting for the uniaxial behavior of the system; it reads

$$H = \sum_{m<n} J_{mn} \mathbf{s}_m \cdot \mathbf{s}_n + d \sum_{m=5}^{12} s_{zm}^2, \quad (1)$$

where the pairs of ions included in the first sum are indicated in Fig. 1(a) and zero-field splitting terms are considered only on the eight highly anisotropic Mn^{3+} ions. We have checked that more-complex choices for the anisotropic term (e.g., small nonaxial terms or higher-order contributions) do not significantly affect the determination of exchange constants and are here neglected for simplicity

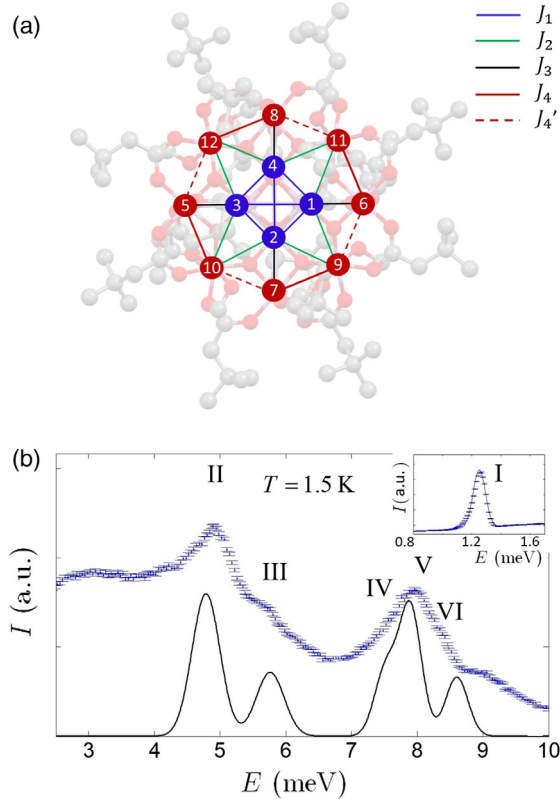


FIG. 1. (a) Scheme of the Mn_{12} -*t*BuAc molecule, with different lines representing the relevant different exchange interactions (J_1 : pairs 1–4, 1–3 and equivalent; J_2 : pair 1–11 and equivalent; J_3 : pair 1–6 and equivalent; J_4 : pair 6–11 and equivalent; J_4' : pair 11–8 and equivalent). Red circles (ions 5–11): Mn^{3+} ions ($s = 2$). Blue circles (ions 1–4): Mn^{4+} ions ($s = 3/2$). Seven distinct exchange constants are allowed by the S_4 symmetry of the molecule, but most models assume only four parameters (J_{1-4} with $J_4' = J_4$) because of similarities in some exchange paths. (b) INS spectrum collected on LET at 1.5 K, using 15.4 meV (4.2 meV in the inset) incident neutron energy. The continuous line is the corresponding simulation with the best-fit parameters (in meV) $J_1 = -1.2$, $J_2 = 3.2$, $J_3 = 6.6$, $J_4 = 0.55$, $J_4' = 0.30$, $d = -0.315$. Eigenstates are listed in Table S1 [26]. Peak I corresponds to a transition between states $M = \pm 10$ and $M = \pm 9$ of the ground $S = 10$ multiplet. The slight asymmetry of the peak is due to the instrumental resolution function of the time of flight spectrometer. Peaks II–VI are intermultiplet transitions to different excited $S = 9$ multiplets. The broad peak at 3 meV is a phonon, as demonstrated by the monotonic increase as Q^2 of the associated form factor.

[26]. As stated above, a firm set of parameters for Eq. (1) could not yet be found. Indeed, the known excitation energies [39] only provide a coarse characterization of the spin Hamiltonian through its eigenvalues. In particular, they lack the selective information associated with the structure of eigenvectors, i.e., how individual atomic spins move when excitations are triggered. Here we use the four-dimensional inelastic neutron scattering (4D-INS) technique [8] to extract such information for the low-energy

transitions shown in Fig. 1(b). The power of the technique comes from the capability to measure the scattering cross section $S(E, \mathbf{Q})$ over large portions of the energy wave-vector (E, \mathbf{Q}) space, yielding a faithful portrayal of spin fluctuations on the space and time scales characterizing the internal dynamics of the magnetic core. This experimental information fingerprints the eigenstates of the spin Hamiltonian, thus enabling us to fix the value of exchange couplings univocally. We have studied specifically Mn_{12} -*t*BuAc, full formula $\{\text{Mn}_{12}\text{O}_{12}[\text{O}_2\text{CCD}_2\text{C}(\text{CD}_3)_3]_{16}(\text{CD}_3\text{OD})_4\} \cdot (\text{C}_2\text{H}_5)_2\text{O}$, which crystallizes with S_4 symmetry, and it is the deuterated analog of the isostructural $[\text{Mn}_{12}\text{O}_{12}(\text{O}_2\text{CCH}_2\text{Bu}')_{16}(\text{MeOH})_4] \cdot \text{MeOH}$ molecule [26,40]. Measurements have been performed on the high-resolution LET spectrometer at ISIS [41], on a collection of oriented single crystals [26]. Figure 1(b) shows INS spectra taken at $T = 1.5$ K with five peaks clearly distinguishable between 1 and 10 meV. Previous INS studies of related Mn_{12} molecules [39] have assigned these peaks to transitions from the ground spin doublet $|S = 10, M = \pm 10\rangle$ (S is the total-spin quantum number), as the population of any other state is negligible at this temperature. For example, the lowest-energy peak (labeled I) at 1.25 meV represents the intramultiplet transition to the $|S = 10, M = \pm 9\rangle$ doublet. Using the 4D-INS technique we can obtain far more information (Fig. 2). The data reported in Fig. 2(a) directly demonstrate [see the discussion of Fig. 3(e) below] that excitation I corresponds to a precession of the giant spin around the anisotropy axis, with its internal structure kept rigid. As discussed in [42] and in [26], this information is equivalent to that contained in the distribution of the giant-spin moment over different Mn ions, i.e., the set of expectation values $\pm\mu_n = \langle S = 10, M = \pm 10 | s_{zn} | S = 10, M = \pm 10 \rangle$. The measured form factor (i.e., the \mathbf{Q} dependence of the scattering intensity) of Fig. 2(a) enables us to extract the set of μ_n values in the inset, which are in line with those determined by neutron diffraction [43] and NMR [44]. The moment distribution reveals ferromagnetic correlations among the four Mn^{4+} and among the eight Mn^{3+} spins, with the two sets antiferromagnetically correlated to each other. However, the Mn^{3+} and Mn^{4+} moments are significantly below saturation, indicating that the spins are not locked in a maximally aligned state due to quantum fluctuations (see Table S1 in [26]).

The local distribution of moments, μ_n , is stable over a range of exchange constants and, hence, is not sufficient to fix the magnitude of the exchange interactions J_{mn} uniquely. It is intuitively clear that exchange is probed more effectively through excitations that break the internal alignment of Mn spins in their ground state. In fact, just like for spin waves in bulk magnetic compounds, their energies and structure directly reflect the values of exchange

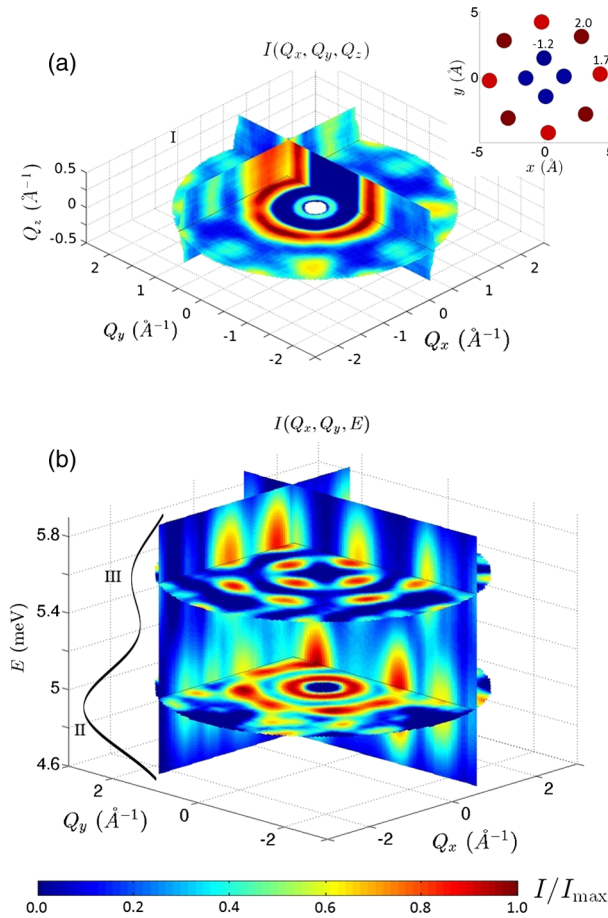


FIG. 2. (a) Form factor for the intramultiplet transition $|S = 10, M = \pm 10\rangle \rightarrow |S = 10, M = \pm 9\rangle$, i.e., $S(E, \mathbf{Q})$ for $E = 1.25$ meV (giant-spin excitation I). The inset shows the equivalent real-space information, that is, the distribution of the static magnetization of the giant spin over the three inequivalent Mn sites, $\mu_n = \langle S = 10, M = 10 | S_{zn} | S = 10, M = 10 \rangle$. The values $\mu_1 = -1.2(2)$, $\mu_6 = 1.7(0.15)$, and $\mu_{11} = 2(0.15)$ are extracted directly from the form factor and compare well with polarized neutron diffraction $(-1.17, 1.84, 1.90)$ [43] and NMR $(-1.3, 1.8, 1.8)$ [44] data on a slightly different variant of Mn_{12} . (b) $S(E, \mathbf{Q})$ as a function of Q_x , Q_y , and E , and integrated over the full Q_z range [45]. The energy window contains the intermultiplet peaks II and III of Fig. 1(b).

constants. These excitations correspond to peaks II–VI in Fig. 1(b) and represent intermultiplet transitions between the ground $|S = 10, M = \pm 10\rangle$ doublet and a set of excited $|S = 9, M = \pm 9\rangle$ doublets. Although these \mathbf{Q} -integrated energy spectra, together with susceptibility (Fig. S2 in [26]), provide constraints on the set of exchange constants, they are not selective. Conversely, a clear identification of the $|S = 9\rangle$ wave functions is achieved thanks to the measured \mathbf{Q} dependencies, which contain detailed information on the composition and symmetry of the states involved in the transition. For example, Fig. 2(b) shows $S(E, \mathbf{Q})$ as a function of Q_x , Q_y , and E , and integrated over the full Q_z range. The energy interval spans peaks

II and III of Fig. 1(b), whereas constant-energy cuts of $S(E, \mathbf{Q})$ for E corresponding to all the peaks in Fig. 1(b) are shown in Fig. 3. The great amount of information available in these experimental data is immediately evident. The $S(E, \mathbf{Q})$ data fully characterize the low-lying multiplets, and make it possible to identify the five exchange parameters. The simulation of these data [Fig. 3(c)] unequivocally establishes the five exchange parameters (in meV): $J_1 = -1.2(1)$, $J_2 = 3.2(2)$, $J_3 = 6.6(3)$, $J_4 = 0.55(5)$, $J'_4 = 0.30(5)$. The agreement between calculation and experiment is very good and the model also fits the magnetic susceptibility (Fig. S2 in [26]) and peak positions [Fig. 1(b)]. There is just a slight discrepancy for the position of peak VI, whose fine-tuning requires additional small parameters in Eq. (1) [26]. As expected in broad terms from the internal structure of the giant spin [Fig. 2(a)], antiferromagnetic couplings between Mn^{3+} and Mn^{4+} ions are leading. The coupling between the four Mn^{4+} ions is ferromagnetic, whereas that between the eight Mn^{3+} ions is weakly antiferromagnetic.

The information on eigenstates is so rich that even subtle variations of exchange parameters alter these maps. For instance, a single parameter is usually assumed for the external Mn^{3+} ring, i.e., $J_4 = J'_4$ in Fig. 1(a). Although these constants are an order of magnitude smaller than the leading ones, by enabling $J_4 \neq J'_4$ we can quantify them separately [26]. The effect of the difference $J_4 - J'_4$ stands out in Fig. 3, showing also [panel (d)] simulations obtained with $J_4 = J'_4 = 0.42$ meV. The intensity distribution in the intermultiplet maps is noticeably different, reflecting a change in composition of the excited $S = 9$ multiplets. It is worth noting that small model variations of this type have significant impact on these maps, but negligible effects on the energy spectrum and susceptibility.

The information on eigenstates collected in reciprocal (E, \mathbf{Q}) space can be made intuitive by using an equivalent description in terms of time and position variables, i.e., by portraying the precession of the 12 Mn spins associated with each excitation. Indeed, the \mathbf{Q} dependence of a peak at energy E_p reflects the spatial pattern of the spins precessing around z with frequency E_p/h , after a resonant perturbation has brought a molecule from its $M = 10$ ground state into a superposition state with a small component on the corresponding excited $M = 9$ state [26]. These precession motions are in a one-to-one correspondence with the form factor $S(E_p, \mathbf{Q})$, as both are set by the same reduced matrix elements [26]. For a generic weak perturbation (e.g., a δ pulse), the resulting motion will then be a weighted superposition of these single-frequency contributions.

Precession patterns, directly extracted from experimental data, are shown in Fig. 3(e) and represent the molecular counterpart of spin-wave excitations in bulk ferromagnets. The difference in the spin dynamics associated to the various transitions is evident: in transition I all the spins

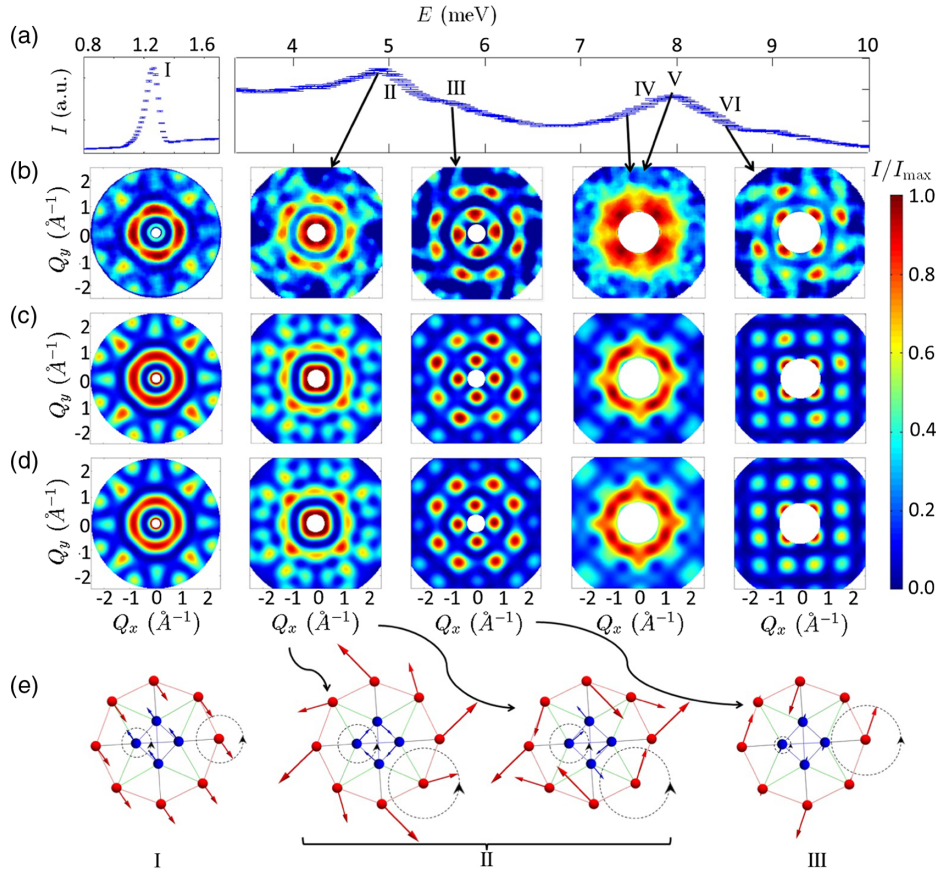


FIG. 3. (a) INS energy spectrum [same as Fig. 1(b)]. (b) Constant-energy cuts for $S(E, \mathbf{Q})$, integrated over the full Q_z range, obtained from measurements at $T = 1.5$ K for incident neutron energies of 4.2 meV (first column, peak I) and 15.4 meV (peaks II–VI) [45]. Each map is normalized to its maximum. (c) Corresponding simulated maps, obtained with parameters (in meV) $J_1 = -1.2(1)$, $J_2 = 3.2(2)$, $J_3 = 6.6(3)$, $J_4 = 0.55(5)$, $J'_4 = 0.30(5)$, $d = -0.315(2)$. Eigenstates are listed in Table S1 [26]. Row (d) highlights the effect of a slight variation of exchange parameters ($J_4 = J'_4 = 0.42$ meV is assumed). Peaks IV and V are too close in energy to extract individual maps, and only their sum is addressed. (e) Precession pattern of the individual Mn spins for excitations I, II, and III. For each excitation, arrows represent the 12 vectors $(\langle s_{xn}(t) \rangle, \langle s_{yn}(t) \rangle)$ describing the spatial pattern of the spins preceding around z , after a resonant perturbation has brought a molecule from its $M = 10$ ground state into a superposition state with a small component on the corresponding excited $M = 9$ state. All the spins precess with the same frequency E/h and dashed circular arrows indicate the direction of the spin precessions for two representative sites. Preparing the system in an initial state with opposite M would induce an opposite precession of the spins. The two panels for excitation II correspond to a pair of degenerate states (Table S1 [26]). For peaks IV, V, and VI, experimental form factors are more noisy or unresolved. Their precession pattern is not directly deduced from data, and is obtained by simulations of the best-fit Hamiltonian (Fig. S5 in [26]).

rigidly precess conserving the same total-spin modulus of the ground state, as expected for a giant spin excitation. Conversely, for all other peaks there is no precession of the total spin, demonstrating the intermultiplet nature of the transitions. In addition, the different symmetries of the excited states (Table S1, [26]) produce clear signatures.

The present results characterize the exchange interactions in Mn_{12} , enabling us to draw for the first time a sound picture of the eigenstates beyond the giant-spin model. This will be the starting point to address important issues in the understanding of this molecule, which are still not really solved after more than 20 years of research. For instance, the relaxation dynamics of Mn_{12} should be influenced by the low-lying excited multiplets, partially

overlapping with the ground one (e.g., these lead to additional relaxation and tunneling pathways with respect to the giant-spin model). In general, these results open remarkable perspectives in understanding nanomagnets with complex polycentric core. These are still relatively little explored and understood but are of fundamental importance, with potential applications in the longer term. We mention, among others, molecules where the role of anisotropy is not perturbative, like in presence of Co [46] or f -electron ions [18]. These can convey their large anisotropy through exchange to the whole core, thus producing large anisotropy barriers or exotic magnetic states (e.g., toroidal or chiral). On the opposite side, we mention small-anisotropy molecules where the set of

exchange couplings results in frustration, which is important both for fundamental and applicative issues [16]. More generally, experiments such as the present one show that 4D-INS is an unrivaled tool for characterizing magnetic clusters where the size and complexity of the spin structure make the interpretation by more conventional routes impossible or ambiguous.

We gratefully acknowledge Peixun Li and James Tellam for the preparation of deuterated products and David Voneshen for the support on LET. A. C., S. C., E. G., G. A., and P. S. acknowledge financial support from the FIRB Project No. RBFR12RPD1 and PRIN Project 2015 No. HYFSRT of the MIUR (I). A. C. acknowledges “Fondazione Angelo Della Riccia” for financial support. G. T., I. J. V.-Y., and R. E. P. W. thank the EPSRC (UK) for support, including funding for an x-ray diffractometer (Grant No. EP/K039547/1).

-
- [1] R. Sessoli, D. Gatteschi, A. Caneschi, and M. A. Novak, *Nature (London)* **365**, 141 (1993).
- [2] L. Thomas, F. Lioni, R. Ballou, D. Gatteschi, R. Sessoli, and B. Barbara, *Nature (London)* **383**, 145 (1996).
- [3] J. M. Hernandez, X. X. Zhang, F. Luis, J. Bartolomé, J. Tejada, and R. Ziolo, *Europhys. Lett.* **35**, 301 (1996).
- [4] M. N. Leuenberger and D. Loss, *Nature (London)* **410**, 789 (2001).
- [5] S. Thiele, F. Balestro, R. Ballou, S. Klyatskaya, M. Ruben, and W. Wernsdorfer, *Science* **344**, 1135 (2014).
- [6] M. Shiddiq, D. Komijani, Y. Duan, A. Gaita-Ariño, E. Coronado, and S. Hill, *Nature (London)* **531**, 348 (2016).
- [7] C. Cervetti, A. Rettori, M. G. Pini, A. Cornia, A. Repolles, F. Luis, M. Dressel, S. Rauschenbach, K. Kern, M. Burghard, and L. Bogani, *Nat. Mater.* **15**, 164 (2016).
- [8] M. L. Baker, T. Guidi, S. Carretta, J. Ollivier, H. Mutka, H. U. Güdel, G. A. Timco, E. J. L. McInnes, G. Amoretti, R. E. P. Winpenny, and P. Santini, *Nat. Phys.* **8**, 906 (2012).
- [9] W. Wernsdorfer and R. Sessoli, *Science* **284**, 133 (1999).
- [10] W. Wernsdorfer, M. Murugesu, and G. Christou, *Phys. Rev. Lett.* **96**, 057208 (2006).
- [11] S. Carretta, T. Guidi, P. Santini, G. Amoretti, O. Pieper, B. Lake, J. van Slageren, F. El Hallak, W. Wernsdorfer, H. Mutka, M. Russina, C. J. Milios, and E. K. Brechin, *Phys. Rev. Lett.* **100**, 157203 (2008).
- [12] A. Furrer and O. Waldmann, *Rev. Mod. Phys.* **85**, 367 (2013).
- [13] J. Luzon, K. Bernot, I. J. Hewitt, C. E. Anson, A. K. Powell, and R. Sessoli, *Phys. Rev. Lett.* **100**, 247205 (2008).
- [14] L. Ungur, S. K. Langley, T. N. Hooper, B. Moubaraki, E. K. Brechin, K. S. Murray, and L. Chibotaru, *J. Am. Chem. Soc.* **134**, 18554 (2012).
- [15] E. Garlatti, T. Guidi, S. Ansbro, P. Santini, G. Amoretti, J. Ollivier, H. Mutka, G. A. Timco, I. Vitorica-Yrezabal, G. Whitehead, R. E. P. Winpenny, and S. Carretta, *Nat. Commun.* **8**, 14543 (2017).
- [16] C. Schröder, H.-J. Schmidt, J. Schnack, and M. Luban, *Phys. Rev. Lett.* **94**, 207203 (2005).
- [17] S. Carretta, P. Santini, G. Amoretti, T. Guidi, J. R. D. Copley, Y. Qiu, R. Caciuffo, G. A. Timco, and R. E. P. Winpenny, *Phys. Rev. Lett.* **98**, 167401 (2007).
- [18] M. S. Dutkiewicz, J. H. Farnaby, C. Apostolidis, E. Colineau, O. Walter, N. Magnani, M. Gardiner, J. B. Love, N. Kaltsoyannis, R. Caciuffo, and P. L. Arnold, *Nat. Chem.* **8**, 797 (2016).
- [19] V. V. Mazurenko, Y. O. Kvashnin, F. Jin, H. A. De Raedt, A. I. Lichtenstein, and M. I. Katsnelson, *Phys. Rev. B* **89**, 214422 (2014).
- [20] S. G. Tabrizi, A. V. Arbutnikov, and M. Kaupp, *J. Phys. Chem. A* **120**, 6864 (2016).
- [21] O. Hanebaum and J. Schnack, *Phys. Rev. B* **92**, 064424 (2015).
- [22] R. Caciuffo, G. Amoretti, A. Murani, R. Sessoli, A. Caneschi, and D. Gatteschi, *Phys. Rev. Lett.* **81**, 4744 (1998).
- [23] I. Mirebeau, M. Hennion, H. Casalta, H. Andres, H. U. Güdel, A. V. Irodova, and A. Caneschi, *Phys. Rev. Lett.* **83**, 628 (1999).
- [24] *Molecular Magnetic Materials: Concepts and Applications*, edited by B. Sieklucka and D. Pinkowicz (Wiley-VCH, Weinheim, Germany, 2017).
- [25] A.-L. Barra, A. Caneschi, A. Cornia, D. Gatteschi, L. Gorini, L.-P. Heiniger, R. Sessoli, and L. Sorace, *J. Am. Chem. Soc.* **129**, 10754 (2007).
- [26] See Supplemental Material at <http://link.aps.org/supplemental/10.1103/PhysRevLett.119.217202>, which includes Refs. [27–38], for details on synthesis, crystallography, neutron scattering experiments, and calculations.
- [27] G. M. Sheldrick, *Acta Cryst.* **C71**, 3 (2015).
- [28] O. V. Dolomanov, L. J. Bourhis, R. J. Gildea, J. A. K. Howard, and H. Puschmann, *J. Appl. Crystallogr.* **42**, 339 (2009).
- [29] R. A. Ewings, A. Buts, M. D. Le, J. van Duijn, I. Bustinduy, and T. G. Perring, *Nucl. Instrum. Methods Phys. Res., Sect. A* **834**, 132 (2016).
- [30] B. S. Tsukerblat, *Group Theory in Chemistry and Spectroscopy. A Simple Guide to Advanced Usage* (Academic Press, London, 1994).
- [31] R. Schnalle and J. Schnack, *Phys. Rev. B* **79**, 104419 (2009).
- [32] O. Waldmann, *Phys. Rev. B* **61**, 6138 (2000).
- [33] O. Waldmann, *Phys. Rev. B* **65**, 024424 (2001).
- [34] J. Jaklic and P. Prelovsek, *Phys. Rev. B* **49**, 5065 (1994).
- [35] J. Jaklic and P. Prelovsek, *Adv. Phys.* **49**, 1 (2000).
- [36] J. Schnack and O. Wendland, *Eur. Phys. J. B* **78**, 535 (2010).
- [37] J. Schnack and C. Heesing, *Eur. Phys. J. B* **86**, 46 (2013).
- [38] P. Prelovsek, in *The Physics of Correlated Insulators, Metals and Superconductors*, edited by E. Pavarini, E. Koch, R. Scalettar, and R. Martin (Verlag des Forschungszentrum Jülich, Jülich, 2017), Vol. 7, Chap. 7.
- [39] G. Chaboussant, A. Sieber, S. Ochsenein, H.-U. Güdel, M. Murrie, A. Honecker, N. Fukushima, and B. Normand, *Phys. Rev. B* **70**, 104422 (2004).
- [40] C. Lampropoulos, M. Murugesu, A. G. Harter, W. Wernsdorfer, S. Hill, N. S. Dalal, A. P. Reyes, P. L. Kuhns, K. A. Abboud, and G. Christou, *Inorg. Chem.* **52**, 258 (2013).

- [41] R. I. Bewley, J. W. Taylor, and S. M. Bennington, *Nucl. Instrum. Methods Phys. Res., Sect. A* **637**, 128 (2011).
- [42] O. Waldmann, R. Bircher, G. Carver, A. Sieber, H. U. Güdel, and H. Mutka, *Phys. Rev. B* **75**, 174438 (2007).
- [43] R. A. Robinson, P. J. Brown, D. N. Argyriou, D. N. Hendrickson, and S. M. J. Aubin, *J. Phys. Condens. Matter* **12**, 2805 (2000).
- [44] Y. Furukawa, K. Watanabe, K. Kumagai, F. Borsa, and D. Gatteschi, *Phys. Rev. B* **64**, 104401 (2001).
- [45] We have exploited the fourfold symmetry of the maps and summed together the cross sections obtained for wave vectors equivalent by rotations, in order to improve data statistics (see also [26]).
- [46] M. Murrie, *Chem. Soc. Rev.* **39**, 1986 (2010).